J Mater Sci (2024) 59:10220–10231

Chemical routes to materials

A new route to electrochemical exfoliation of borophene for scalable production

Duygu Kuru[1,*] and Cihan Kuru[2]

[1] Department of Chemical Engineering, Bilecik Seyh Edebali University, Bilecik 11100, Turkey
[2] Department of Metallurgical and Materials Engineering, Bilecik Seyh Edebali University, Bilecik 11100, Turkey

Received: 16 January 2024
Accepted: 10 May 2024
Published online: 29 May 2024

ABSTRACT

Scalable production of freestanding borophene is of great importance for practical applications. Top-down approaches such as sono-chemical and electrochemical exfoliation are challenging due to complex structure and low electrical conductivity of boron. In this study, we envisaged to add multiwalled carbon nanotubes (MWCNTs) into boron powder to tackle the low conductivity of boron. A few layer borophene sheets down to 0.8 nm thickness were successfully prepared by anodic exfoliation of crystalline boron powder in Na_2SO_4. + 20 V was found to be the optimum exfoliation voltage as it results in thinner and larger sheets compared to higher voltage values. More than 50% of the exfoliated sheets are less than 10 layers, which indicate the potential of the process for freestanding borophene production. After the exfoliation process, MWCNTs could be effectively removed by a toluene/water system and subsequent filtration through a cellulose membrane. The method proposed here is scalable because the amount of boron powder that can be exfoliated can be increased without a limit as long as sufficient amount of MWCNTs are added to provide enough electrical conductivity. This novel strategy can also be extended to exfoliate other low conductivity materials, promoting future research.

Handling Editor: Maude Jimenez.

Address correspondence to E-mail: duygu.gokdai@bilecik.edu.tr

https://doi.org/10.1007/s10853-024-09769-0

GRAPHICAL ABSTRACT

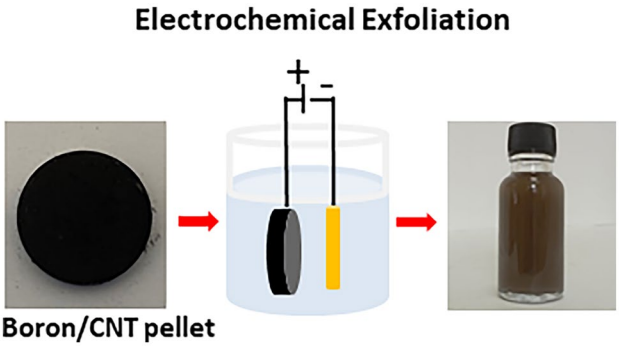

Introduction

Two-dimensional (2D) materials have been the center of great interest in the last two decades for their unique properties, which arise from quantum confinement effect. Recently, elemental 2D materials have emerged including silicene, phosphorene, antimonene, stanene, bismuthene, germanene, tellurene and borophene [1–8]. Among them, borophene, 2D allotrope of boron, exhibits anisotropic behavior and polymorphism with some interesting mechanical, chemical and electronic properties due to its diversified bonding structure [9]. Theoretically, borophene has been predicted to have high carrier mobility [10], catalytic activity [11], elastic modulus [12] and lithium/sodium storage capacity [13], which makes it promising for electronics, energy storage, catalysis and mechanical applications.

Initial experimental efforts to realize borophene have mainly focused on the synthesis on various metal substrates by atomic layer deposition (ALD), molecular beam epitaxy (MBE) and chemical vapor deposition (CVD) [12, 14, 15]. However, these methods require low pressure conditions, are not scalable and some of the precursors used in these methods are highly toxic. For practical applications, scalable production of freestanding borophene is crucial. Top-down approaches such as sono-chemical exfoliation or electrochemical exfoliation are suitable methods to produce freestanding borophene. Due to the non-layered structure of boron, exfoliation of boron was believed to be impossible until 2018, when the first experimental demonstration was performed by Li [16]. Li et al. employed sonication assisted liquid exfoliation method, in which bulk boron powder was exfoliated in DMF and IPA to produce few layer boron nanosheets with a concentration of 0.05 and 0.09 mg/mL, respectively. Later, Ranjan et al. reported the sono-chemical exfoliation of boron in DMF, IPA, acetone, water and ethylene glycol (EG) [17]. Among all, only acetone and EG was found to produce single layer borophene while the others led to multilayer sheets. Zhang et al. developed a solvothermal-assisted liquid exfoliation method, in which bulk boron was solvothermally treated in acetone at 200 °C prior to probe sonication [18]. Taking advantage of the swelling effect of acetone, this method produced few layers borophene with significantly improved lateral size up to 5.05 μm. Although sono-chemical exfoliation is a low cost and facile method, the process takes long time, requires high ultrasonic power (> 500 W) and the yield is low. A scalable method based on mechanical exfoliation of boron using ball milling was introduced by Zielinkiewicz et al. who produced gram scale borophene with an average thickness of 5.5 nm [19]. However, ball milling is prone to induce significant structural disorder and contaminations, which can be detrimental to the properties of borophene.

Alternately, electrochemical exfoliation is an effective method to produce 2D materials. So far, graphene, transition metal dichalcogenides (TMDs), black phosphorus, silicene and antimonene nanosheets have been prepared by anodic or cathodic exfoliation, in which intercalation of anions or cations causes the expansion and exfoliation of the bulk material [20–24]. However, the low electrical conductivity of boron hinders its electrochemical exfoliation. To circumvent this problem, Sielicki et al. used amorphous boron which has a lower band gap and squeezed the bulk boron powder into Cu and Ni mesh [25]. Cu and Ni mesh provided

sufficient conductivity for the electrochemical exfoliation of boron powder. Though this method was successful to produce borophene sheets with thicknesses of 3–26 nm, it is not scalable as the amount of boron that could be squeezed into the metal mesh is limited. Larger amount of boron powder would result in thicker electrodes and eventually lead to insufficient conductivity. In another effort, a high temperature electrochemical exfoliation was employed, in which a boron rod was heated to temperatures between 600 and 1000 °C by a heating coil to increase carrier density and thus electrical conductivity [26]. The exfoliated material was subjected to two hours of sonication and centrifuged at 4000 rpm yielding a gray-colored suspension. Yet, electrolyte decomposition is likely to occur and borophene is prone to oxidation at high temperatures as well as no detailed characterization of the obtained product was performed.

Herein, we developed a novel strategy for the electrochemical exfoliation of boron. Boron/multiwalled carbon nanotubes (MWCNTs) composite pressed into a pellet was used as anode for the electrochemical exfoliation of boron in Na_2SO_4. MWCNTs provided the necessary conductivity to the electrode and were successfully removed after the exfoliation process. Unlike the method used by Sielicki et al., there is no limit to the amount of boron that can be exfoliated, which signifies the scalability of the process. We studied the effect of exfoliation voltage on the thickness and lateral size distribution of borophene sheets. Atomic force microscopy (AFM), high resolution transmission electron microscopy (HRTEM), energy-dispersive X-ray spectroscopy (EDX), Raman spectroscopy, X-ray photoelectron spectroscopy (XPS), scanning electron microscopy (SEM), Fourier transform infrared spectroscopy (FTIR), thermogravimetry (TGA), differential scanning calorimetry (DSC) and photoluminescence spectroscopy (PL) measurements were employed to examine the physical and chemical characteristics of borophene.

Methods

Preparation of boron/MWCNTs Pellets

MWCNTs were size purified prior to use by centrifugation of the MWCNTs dispersion in IPA at 2000 rpm, after which the precipitate were collected. 375 mg crystalline boron powder (95–97% purity, Pavezyum) was dispersed in 20 ml deionized (DI) water to which 125 mg MWCNTs (–COOH modified, 15–35 μm length, 18–28 nm diameter, 96% purity, Nanokar) dispersed in isopropyl alcohol (IPA) and 50 mg polymethyl methacrylate (PMMA) (Sigma-Aldrich) dissolved in acetone were added. The mixture was sonicated for 30 min in an ultrasonic bath and then dried at 80 °C overnight. The resulting powder was pressed into a circular pellet having a diameter of 10 mm at 500 bar using a manual hydraulic press. Silver epoxy was spread on the backside of the pellet and then a piece of Cu wire was attached to form an electrical contact. Silicon epoxy was applied on the backside to isolate the contact area.

Electrochemical exfoliation

Two electrode setup was used for the electrochemical exfoliation process, in which the pressed pellet served as the working electrode while Pt coil as the counter electrode. The exfoliation was conducted at + 20, + 30 and + 40 V in 0.5 M Na_2SO_4 to which glycerin was added (1:1 v/v ratio) to increase viscosity. A water bath was used to prevent excess heating. The expended and exfoliated material was washed with DI water several times to remove ionic residues and acetone to remove the PMMA binder in a vacuum filtration system.

Removal of the MWCNTs

The collected powder was redispersed in 200 ml toluene/water system (1:1 v/v ratio) by 30 min of sonication during which the MWCNTs accumulated at the toluene/water interface while borophene sheets remained in the water part. Subsequently, the borophene sheets were collected via a separation funnel, then filtered through a cellulose membrane with a pore size of 8 μm. Finally, borophene dispersion was centrifuged at 4500 rpm for 20 min to remove thick boron particles.

Characterization

TEM samples were prepared by drop casting borophene dispersion on a carbon-coated Cu grid, followed by drying at 50 °C overnight. HRTEM and EDX analyses were performed with FEI TALOS F200S TEM. For AFM measurements, borophene dispersion was spray coated on a SiO_2-coated Si

substrate. AFM measurements were conducted with tapping mode using Hitachi 5100N. Borophene dispersion was drop casted on a piece of Cu foil at 100 °C for Raman and PL measurements, while the dispersion was drop casted on a Si wafer for SEM and XPS measurements. Raman spectroscopy measurements were carried out by WITech alpha 300R spectrophotometer using a laser wavelength of 532 nm and laser power of 5 mW. PL measurements were conducted with Dongwoo Optron spectrophotometer at room temperature in the range of 350–900 nm. The excitation wavelength and power was 325 nm and 200 mW, respectively. XRD measurements were performed on Rigaku D-Max diffractometer using a Cu-Kα source (1.54 Å). XPS data were obtained on SPECS FlexMod system equipped with a Al-Kα radiation source (1486.71 eV). SEM/EDX data were acquired on a Zeiss Sigma 300 SEM. FTIR spectra were obtained by PERKIN ELMER/SPECTRUM 100 spectrometer using KBr pellet and ATR (attenuated total reflection) techniques. TGA and DSC analysis were performed by NETZSCH STA 449 F1 under air atmosphere. For the measurements, about 5 mg of borophene powder was placed in an alumina crucible and heated up to 800 °C with a rate of 10 °C min^{-1}. The flow rate of air was kept constant at 40 ml min^{-1}.

Results and discussion

The production process of borophene sheets is illustrated in Fig. 1. Our starting material is crystalline boron powder whose particle size spans from 200 nm to 3 μm (Fig. S1). The XRD pattern of the boron powder (Fig. S2) matches well with β-rhombohedral boron with 105 atom per unit cell (B_{105}-PDF# 01–072-1705). As boron itself has low electrical conductivity, it can't be electrochemically exfoliated at room temperature. In order to circumvent this problem, boron powder was mixed with MWCNTs with a weight ratio of 3:1 (Fig. 1a) and pressed into a pellet form (Fig. 1b). PMMA binder was employed to ensure the adhesion between boron powder and MWCNTs. The resistance between two sides of the pellet was in the range of 50–100 Ω, which was sufficient for the electrochemical exfoliation. MWCNTs were chosen based on its high electrical conductivity and chemical stability. Alternatives like graphite or metal powders would undergo exfoliation or dissolution under anodic conditions causing impurities and reducing the efficiency of the process by drawing significant amount of current.

Boron was anodically exfoliated in a two electrode set up, where a mixture of Na_2SO_4 and glycerin was used as the electrolyte (Fig. 1c). Adding glycerin to the electrolyte increased the viscosity and slowed down water decomposition reaction enabling the complete exfoliation of the pellet electrode. When glycerin not used, exfoliation process was terminated by the early rupture of the electrode due to aggressive oxygen gas evolution. The exfoliation was conducted under different voltage values to investigate the effect of voltage. + 10 V was insufficient to drive the exfoliation of boron because only a few expanded pieces emerged after 2 h. At higher voltages (+ 20, + 30 and + 40 V), electrode shows a notable expansion, which is followed by simultaneous break-off into expanded pieces and exfoliation of borophene sheets as evident by the dark brown cloud formed on top of the electrolyte (Fig. 2). The current initially increases to roughly double then slowly decreases to zero, which hints that initial current increase is resulted from the increased surface area due to the expansion of boron while the subsequent decrease can be attributed to reduced surface area as the electrode breaks off and the exfoliation of borophene takes place. Increasing the voltage form + 20 to + 40 V increased the initial current value from 290 to 900 mA and the peak current value from 420 mA to 1.6 A. As a result, exfoliation

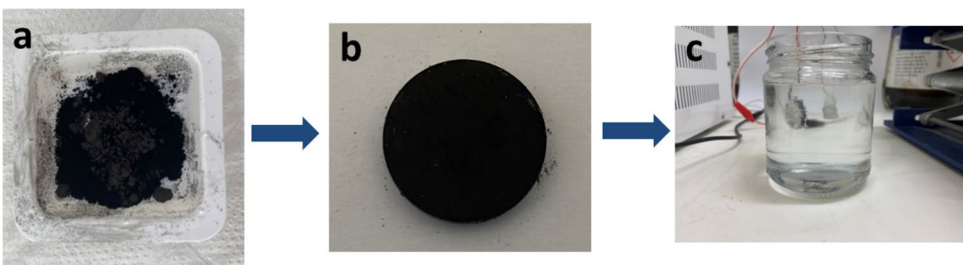

Figure 1 Photographs of **a** crystalline boron powder and MWCNTs mixture, **b** boron/MWCNTs pellet and **c** electrochemical exfoliation setup used for borophene production.

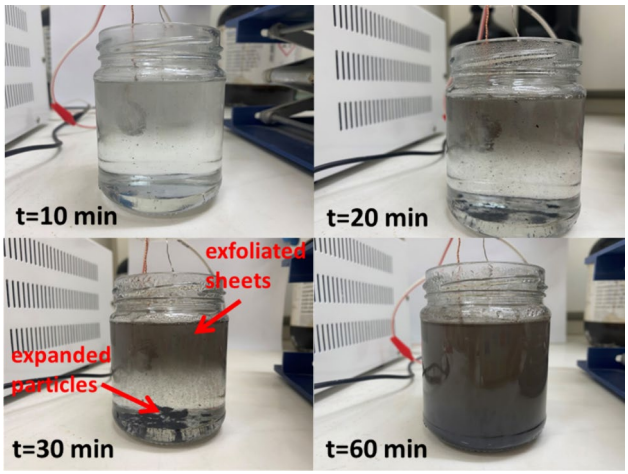

Figure 2 Snapshots of the electrochemical exfoliation process taken at different time intervals.

time decreased from 105 to 20 min. Larger current leads to faster electrochemical reactions resulting in shorter exfoliation time. Anodic exfoliation of boron occurs in three stages [27]. First, free radicals (·OH, ·O) generated by the oxidation of water molecules attack the edges of boron particles unzipping the edge sites. Second, free radicals and SO_4^{2-} anions intercalate positively charged boron through the edge sites causing its expansion. Third, radicals and anions undergo an oxidation reaction converting to gaseous species, which force boron lattice to exfoliate producing borophene sheets. LiCl (1 M in DMSO) was also tried as the electrolyte for the exfoliation of boron. The cathodic exfoliation of boron was conducted at -20 V. The exfoliation process prematurely ended after a few minutes due to the rupture of the electrode. A white-greyish layer was noticed on the surface of the electrode (Figure S3), which is attributed to the solid electrolyte interphase (SEI) formed by the decomposition of the electrolyte. As the SEI has low electrical conductivity [28], the exfoliation starts to occur at the back of the electrode causing it to rupture. Hence, we conclude that Na_2SO_4 is a more suitable electrolyte for the exfoliation of boron.

In order to separate MWCNTs from borophene, a two-step separation procedure was employed. In the first step, after washing and collecting the borophene/MWCNTs powder was placed in a toluene/water system (Fig. 3a) and sonicated (Fig. 3b), which led MWCNTs to assemble at the toluene/water interface, while borophene sheets were dispersed in the water part as indicated by the apparent color difference (Fig. 3c). During the sonication, -COOH modified MWCNTs moved to the toluene/water interface with the aid of ultrasonic power to reduce the interfacial tension [29]. Subsequently, the water part was collected with a separation funnel (Fig. 3d and e). In the second step, the collected borophene dispersion was filtered through an 8 μm pore sized cellulose membrane to remove any remaining MWCNTs (Fig. 3f). No vacuum was applied during the filtration and the dispersion was constantly stirred with a glass rod in order to prevent the blockage of the membrane. Otherwise, fast filtration clogs the membrane, lowering the borophene yield. The final product shows the typical brown color of borophene dispersions (Fig. 3g), indicating the success of the separation process. EDX measurements were conducted to quantify the amount of residual MWCNTs in the purified borophene dispersion. For the measurements, borophene dispersion was drop casted on a Si substrate. No carbon could be detected in the EDX spectra of two different regions (Fig. S4a and b), proving that MWCNTs were effectively removed.

AFM measurements were performed to determine the thickness and size distribution of the borophene sheets exfoliated under different voltage values. AFM topographic images, representative height profiles, thickness and lateral size histograms are given in Fig. 4 and Fig. S5. The mean thickness of the borophene sheets exfoliated at + 20 V is 3.9 nm, while exfoliation at + 30 and + 40 V led to larger mean thickness values of 8.7 and 8.6 nm, respectively. Furthermore, + 20 V could yield bilayer sheets whereas the thinnest sheets obtained from + 30 and + 40 V were 4–5 layers. Moreover, the mean lateral size of the borophene sheets exfoliated at + 20 V was 210 nm, which is much larger than those exfoliated at + 30 and + 40 V. The thickness and size distribution of the sheets indicates that exfoliation was more effective at + 20 V most likely because of the fragmentation and incomplete exfoliation at higher voltages due to excess gas release. The lateral size of the sheets are relatively small compared to literature [17, 18, 25], which may be due to the preferential exfoliation of smaller boron particles as they have lower internal resistance. Overall, 40% of the sheets are less than 10 layers, which prove the efficiency of the anodic exfoliation process.

The FTIR spectra of bulk boron and exfoliated borophene samples are compared in Fig. 5a, in which bulk boron and borophene sheets mostly exhibit similar stretching modes. The peaks at 1034, 1227, 2829 and

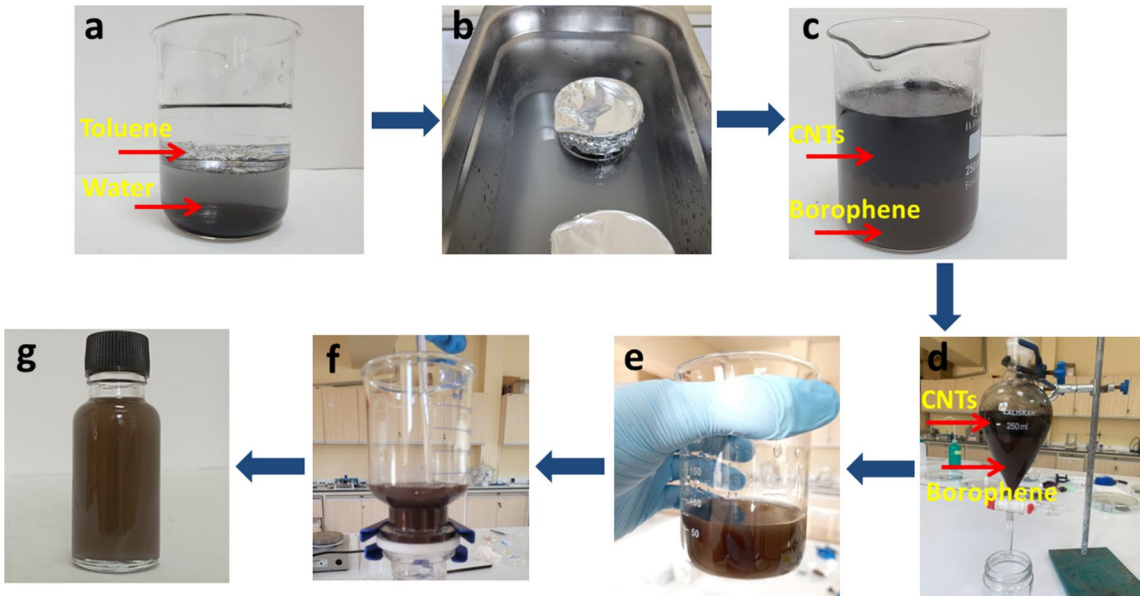

Figure 3 Photographs of the **a** toluene/water system used to separate MWCNTs, **b** sonication step of the borophene/MWCNTs powder in the toluene/water system, **c** MWCNTs and borophene assembled in the toluene and water part, respectively after the sonication, **d** separation funnel used to collect borophene dispersion, **e** collected water part, **f** post filtration of remaining MWCNTs and **g** final borophene dispersion.

2904 cm^{-1} could be identified as B-O-B, B-O, B-B and B-B, respectively [30]. After the exfoliation, new peaks emerged at 1340 and 1554 cm^{-1}, which are attributed to B-O bonds of B_2O_3 [31]. Raman spectroscopy measurements were carried out to investigate the structural properties of borophene. The measurements were taken on a Cu substrate due to its blank Raman spectrum (Fig. S6) and Raman enhancement effect [32]. Figure 5b depicts the Raman spectra of the crystalline boron and borophene. The Raman spectra of the boron and borophene are nearly identical. Borophene exhibits six predominant peaks at 298, 435, 641, 738, 781 and 1084 cm^{-1}, which agree with β boron [33]. Moreover, no Raman features arising from the MWCNTs could be detected, verifying the successful removal of the MWCNTs. The chemical composition of borophene was further investigated by XPS. The XPS survey scan of borophene (Fig. S7a) displays the peaks matching with C, O, B, Ca, S and Si elements. The C peak (Fig. S7b) is the cumulative result of the remaining MWCNTs, residual PMMA and adsorbed hydrocarbon species. The Ca impurities most likely leached from the glass vial during the sonication whereas S was originated from the SO_4 ions attached to borophene. The amount of Ca and S impurities was calculated to be 0.85 and 1.92%, respectively (Table S1). Figure 5c and d show the B 1 s spectra of the crystalline boron and borophene. The XPS spectrum of the crystalline boron can be deconvoluted into two peaks corresponding to B-B (187.6 eV) and B-O bonds of boron suboxide (189.2 eV) [16, 17]. The amount of B–B and B–O bonds were calculated to be 36 and 64%. The large fragment of the B-O bonds suggests the formation of native oxide layer on boron surface, which is typical for commercial boron powders. On the other hand, deconvoluted XPS spectrum of borophene exhibits three peaks located at 187.4, 188.6 and 192.0 eV, which can be assigned to B–B, B–O and B_2O_3 bonds [34] with a content of 56%, 36% and 8%, respectively. The appearance of the boron trioxide peak is most likely due to the electrochemical reactions taking place during the exfoliation. Interestingly, the fragment of B-B bonds is larger for borophene, which could be resulted from the freshly cleaved surface of the borophene sheets after the exfoliation process. Moreover, the total percentage of the oxide bonds in borophene was calculated to be 44%.

HRTEM images presented in Fig. 6a and d depicts a few layer borophene sheets. The close up images show the clear lattice fringes indicating the high crystallinity of the borophene sheets (Fig. 6b and e). The interplanar distance for two different sheets was calculated as 4.6 and 5 Å (Fig. 6c and f), which correspond to (021) and (104) planes of β-rhombohedral crystal structure,

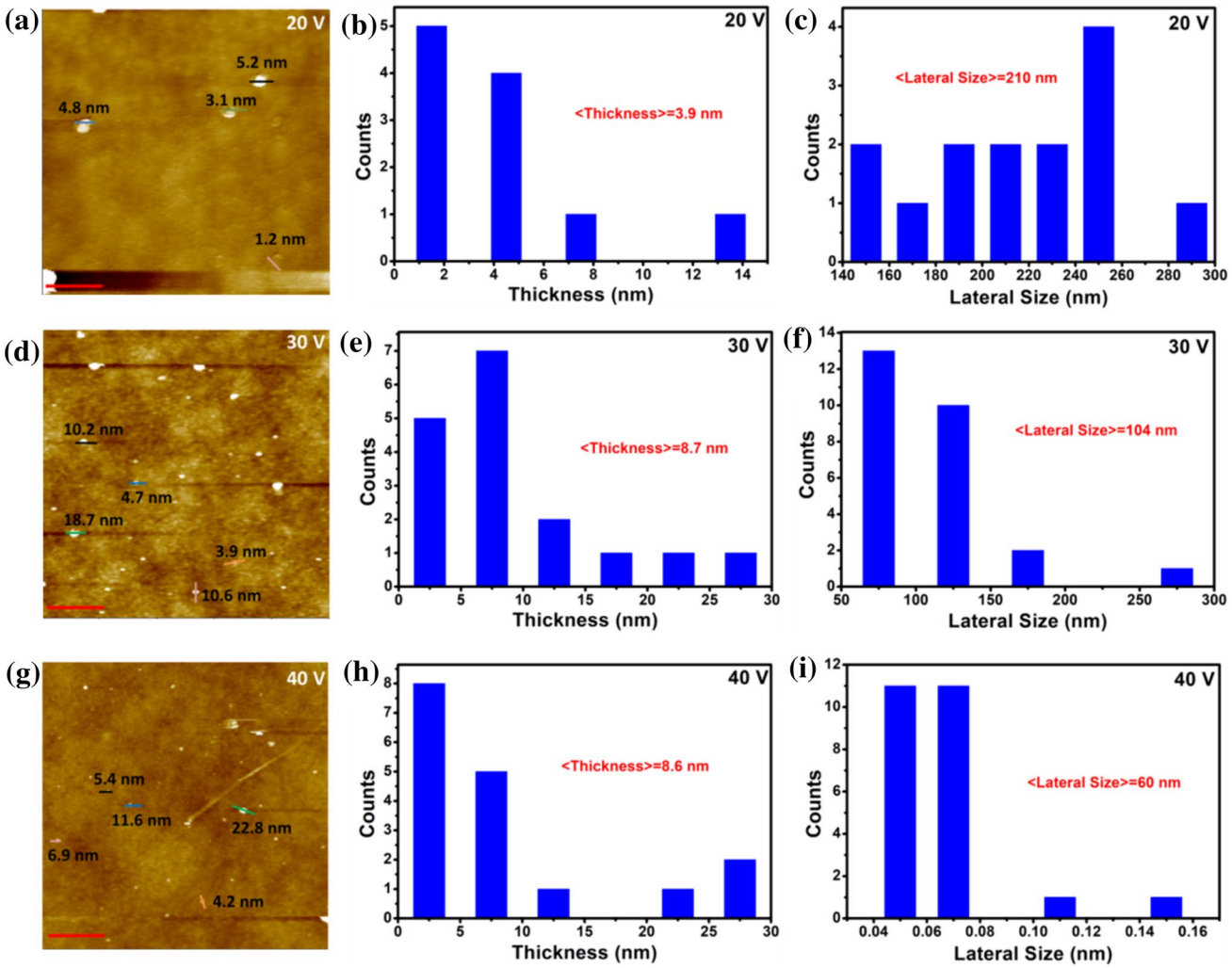

Figure 4 **a**, **d** and **g** AFM topographic images of the borophene sheets exfoliated at + 20 V, + 30 and + 40 V (Scale bar: 1 μm). **b**, **e** and **h**. Thickness histograms and **c**, **f** and **i** lateral size histograms of the corresponding borophene sheets.

respectively (Fig. S2). The EDX analysis confirms the presence of B, O and C elements with an atomic ratio of 42.9, 41.5 and 15.6% (Figure 6g, h, i and j). The O signal arises from the boron suboxide and boron trioxide phases as verified by the XPS results and the C is most likely resulted from the residual PMMA and partially from the TEM grid. Besides, the amount of O was found to be consistent with the XPS results.

Oxidation behavior of borophene in air was investigated by TGA and DSC analysis (Fig. 7a). The weight of borophene powder starts to increase at around 530 °C due to oxidation, which is consistent with the exothermic peak observed in the DSC curve. This data shows that few layer borophene has a fairly good oxidation resistance most likely due to the protective effect of the oxidized outer surface layer. The chemical stability of borophene was assessed by FTIR measurements (Fig. 7b) after soaking borophene powder in 1 M NaOH and 1 M HCl for 24 h. The borophene powder survived in both solutions without any observed dissolution. The borophene powder soaked in NaOH exhibits similar FTIR spectrum with the untreated borophene, showing borophene's chemical stability against NaOH. On the other hand, borophene exhibits a new peak at 3673 cm^{-1} originated from O–H bonding [35] after the HCl treatment and the intensities of the some peaks (460, 73, 852, 1394, 2894 and 2959 cm^{-1}) change, indicating that HCl induced chemical modifications in borophene. The structural stability of borophene at high temperatures was investigated by Raman spectroscopy measurements (Fig. 7c). For the measurements, borophene samples drop casted

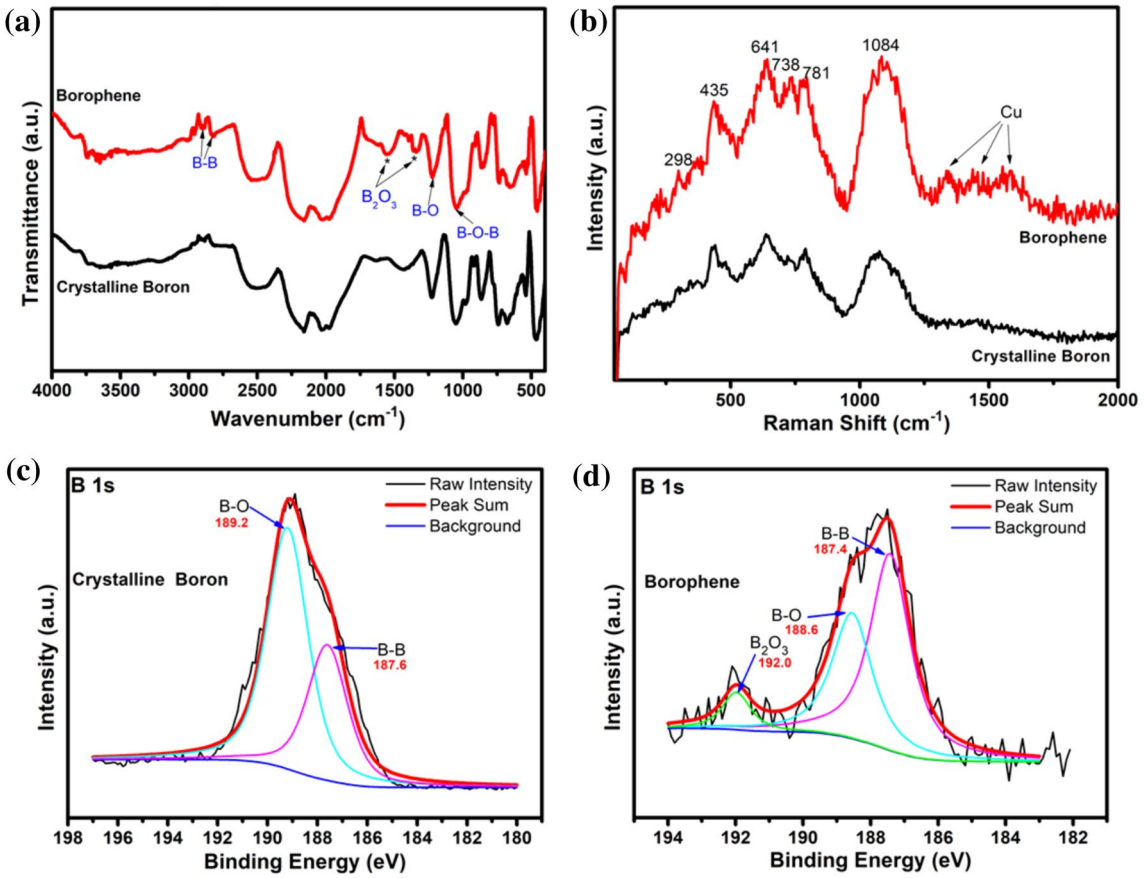

Figure 5 **a** FTIR and **b** Raman spectra of crystalline boron and borophene. B 1 s XPS spectra of **c** crystalline boron and **d** borophene.

on Cu foil were annealed at 600 and 800 °C under N_2 atmosphere for an hour. Annealing borophene at 600 °C did not alter the Raman spectrum significantly, indicating that the structure of borophene was preserved. However, when borophene was annealed at 800 °C, the peaks at 435 and 632 cm^{-1} disappeared whereas two new peaks emerged at 485 and 535 cm^{-1}, implying a structural change. In addition, the peaks become more pronounced, which could be ascribed to enhanced crystallinity. PL measurements were carried out to study the effect of annealing on the electronic structure of borophene. PL spectrum of borophene exhibits two different emission peaks centered at 493 and 610 nm corresponding to band gap values of 2.52 and 2.03 eV. The peaks at 493 and 652 nm are resulted from the exfoliated borophene sheets and unexfoliated boron particles, respectively. The sharp peak at 652 nm is originated from the frequency multiplication of the laser wavelength (325 nm) [36]. After the annealing, the intensity of the PL spectra increases significantly due to enhanced crystallinity. However, there is no obvious shift in the PL maxima, indicating that the electronic band structure of borophene was not modified upon annealing up to 800 °C.

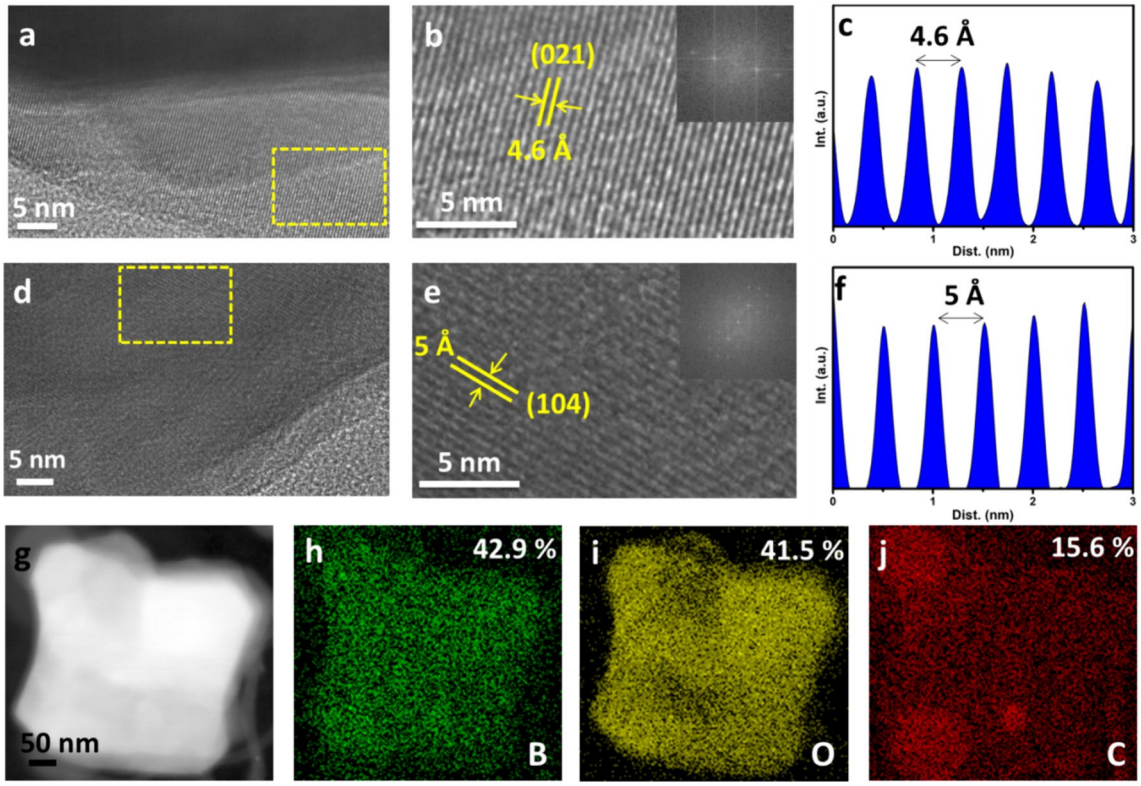

Figure 6 **a** and **d** HRTEM images of two different borophene sheets. **b** and **e** Close up images of the sheets and the corresponding FFT patterns. **c** and **f** Intensity line profiles calculated perpendicular to the lattice fringes. **g** HAADF image of a borophene sheet. EDX mapping images of **h**–**j** B, O and C elements.

Conclusions

In conclusion, we developed a novel approach for the electrochemical exfoliation of boron, in which MWCNTs are utilized to compensate the low conductivity of boron. A few layer borophene sheets could be produced by anodic exfoliation in Na_2SO_4. We studied the effect of voltage on the exfoliation behavior of boron. + 10 V was not sufficient to drive the exfoliation of boron particles. Increasing the voltage from + 20 to + 40 V led to thicker and smaller sheets. Therefore, + 20 V is the optimal voltage value for the exfoliation of boron, resulting in a mean thickness of 3.9 nm and lateral size of 210 nm. The exfoliated borophene sheets are highly crystalline with a β-rhombohedral crystal structure. The total percentage of the oxide bonds slightly increased after the exfoliation of boron, most likely resulted from the electrochemical reactions occurring during the exfoliation process. This process is facile, rapid and scalable and can be adopted to exfoliate other nonconductive materials.

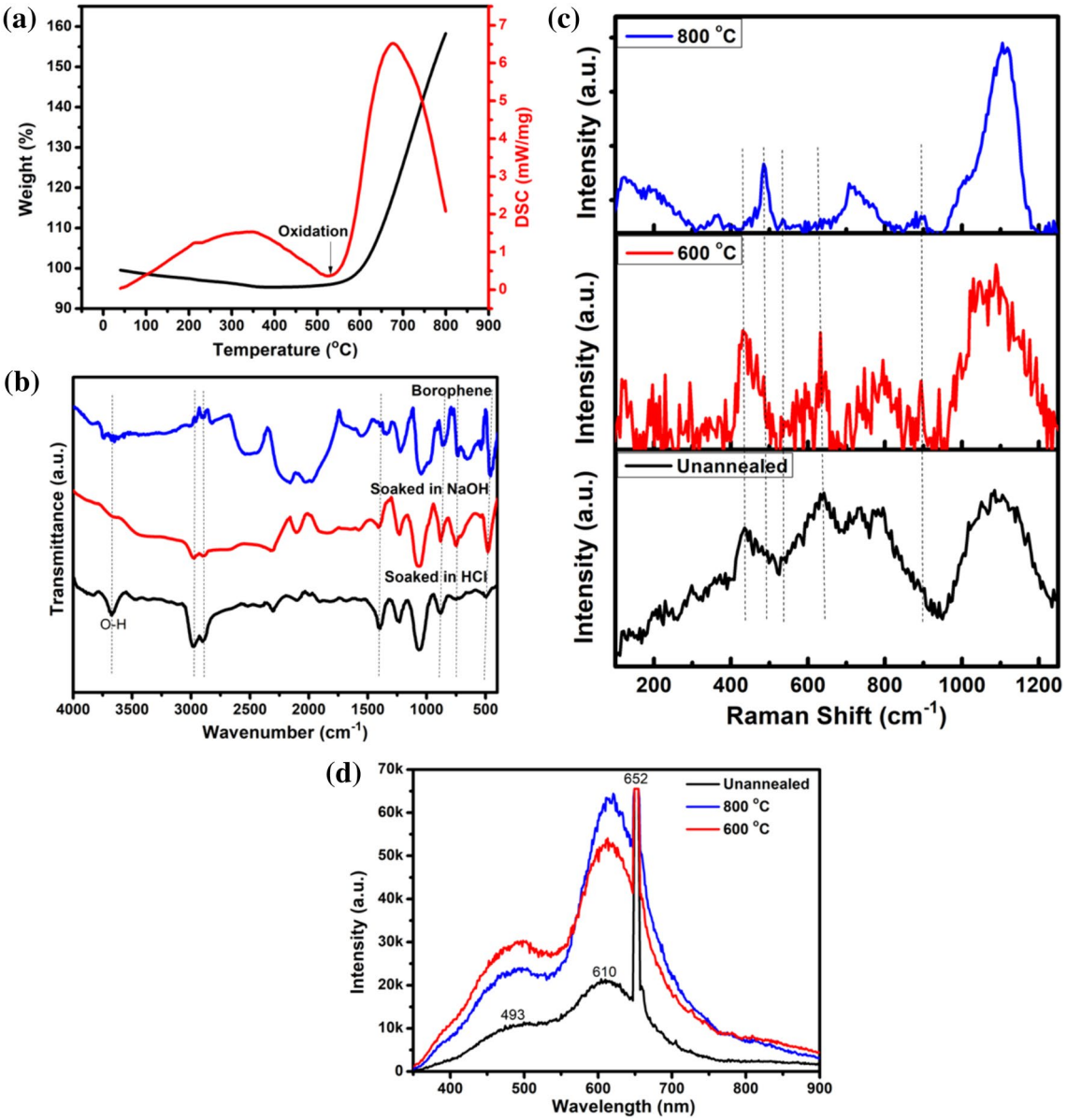

Figure 7 **a** TGA and DSC curves of borophene powder obtained in air atmosphere. **b** FTIR spectra of pristine borophene, borophene soaked in NaOH and borophene soaked in HCl. **c** Raman and **d** PL spectra of unannealed and annealed borophene samples (at 600 and 800 °C in N_2).

Acknowledgements

This work was funded by The Scientific and Technological Research Council of Turkey (Grand No. 222M300).

Author's contribution

All authors have read and approved the manuscript. DK was involved in conceptualization, methodology, and writing of the original draft. CK contributed to methodology, data curation, and writing–reviewing and editing.

Data availability

Raw data will be made available upon reasonable request.

Declarations

Conflict of interest The authors declare that they have no known competing financial interests or personal relationships that could have appeared to influence the work reported in this paper.

Ethical approval Not applicable.

Supplementary Information The online version contains supplementary material available at https://doi.org/10.1007/s10853-024-09769-0.

References

[1] Oughaddou H, Enriquez H, Tchalala MR, Yildirim H, Mayne AJ, Bendounan A, Dujardin G, Ali MA, Kara A (2015) Silicene, a promising new 2D material. Prog Surf Sci 90:46–83. https://doi.org/10.1016/j.progsurf.2014.12.003

[2] Liu H, Neal AT, Zhu Z, Luo Z, Xu X, Tománek D, Ye PD (2014) Phosphorene: an unexplored 2D semiconductor with a high hole mobility. ACS Nano 8:4033–4041. https://doi.org/10.1021/nn501226z

[3] Ji J, Song X, Liu J, Yan Z, Huo C, Zhang S, Su M, Liao L, Wang W, Ni Z, Hao Y (2016) Two-dimensional antimonene single crystals grown by van der Waals epitaxy. Nat Commun 7:13352. https://doi.org/10.1038/ncomms13352

[4] Zhu FF, Chen WJ, Xu Y, Gao CL, Guan DD, Liu CH, Qian D, Zhang SC, Jia JF (2015) Epitaxial growth of two-dimensional stanene. Nat Mater 14:1020–1025. https://doi.org/10.1038/nmat4384

[5] Aktürk E, Aktürk OÜ, Ciraci SJPRB (2016) Single and bilayer bismuthene: Stability at high temperature and mechanical and electronic properties. Phys Rev B 94:014115. https://doi.org/10.1103/PhysRevB.94.014115

[6] Acun A, Zhang L, Bampoulis P, Farmanbar MV, van Houselt A, Rudenko AN, Lingenfelder M, Brocks G, Poelsema B, Katsnelson MI, Zandvliet HJ (2015) Germanene: the germanium analogue of graphene. J Phys Condens Matter 27:443002. https://doi.org/10.1088/0953-8984/27/44/443002

[7] Wang Y, Qiu G, Wang R, Huang S, Wang Q, Liu Y, Du Y, Goddard WA III, Kim MJ, Xu X, Ye PD (2018) Field-effect transistors made from solution-grown two-dimensional tellurene. Nat Electron 1:228–236. https://doi.org/10.1038/s41928-018-0058-4

[8] Mannix AJ, Zhang Z, Guisinger NP, Yakobson BI, Hersam MC (2018) Borophene as a prototype for synthetic 2D materials development. Nat Nanotechnol 13:444–450. https://doi.org/10.1038/s41565-018-0157-4

[9] Hou C, Tai G, Wu Z, Hao J (2020) Borophene: current status, challenges and opportunities. ChemPlusChem 85:2186–2196. https://doi.org/10.1002/cplu.202000550

[10] Li D, Gao J, Cheng P, He J, Yin Y, Hu Y, Chen L, Cheng Y, Zhao J (2020) 2D boron sheets: structure, growth, and electronic and thermal transport properties. Adv Funct Mater 30:1904349. https://doi.org/10.1002/adfm.201904349

[11] Tai G, Xu M, Hou C, Liu R, Liang X, Wu Z (2021) Borophene nanosheets as high-efficiency catalysts for the hydrogen evolution reaction. ACS Appl Mater Interfaces 13:60987–60994. https://doi.org/10.1021/acsami.1c15953

[12] Mannix AJ, Zhou XF, Kiraly B, Wood JD, Alducin D, Myers BD, Liu X, Fisher BL, Santiago U, Guest JR, Yacaman MJ (2015) Synthesis of borophenes: anisotropic, two-dimensional boron polymorphs. Science 350:1513–1516. https://doi.org/10.1126/science.aad108

[13] Jiang HR, Lu Z, Wu MC, Ciucci F, Zhao TS (2016) Borophene: a promising anode material offering high specific capacity and high rate capability for lithium-ion batteries. Nano Energy 23:97–104. https://doi.org/10.1016/j.nanoen.2016.03.013

[14] Feng B, Zhang J, Zhong Q, Li W, Li S, Li H, Cheng P, Meng S, Chen L, Wu K (2016) Experimental realization of two-dimensional boron sheets. Nat Chem 8:563–568. https://doi.org/10.1038/nchem.2491

[15] Tai G, Hu T, Zhou Y, Wang X, Kong J, Zeng T, You Y, Wang Q (2015) Synthesis of atomically thin boron films on copper foils. Angew Chem Int Ed 54:15473–15477. https://doi.org/10.1002/anie.201509285

[16] Li H, Jing L, Liu W, Lin J, Tay RY, Tsang SH, Teo EHT (2018) Scalable production of few-layer boron sheets by liquid-phase exfoliation and their superior supercapacitive performance. ACS Nano 12:1262–1272. https://doi.org/10.1021/acsnano.7b07444

[17] Ranjan P, Sahu TK, Bhushan R, Yamijala SS, Late DJ, Kumar P, Vinu A (2019) Freestanding borophene and its hybrids. Adv Mater 31:1900353. https://doi.org/10.1002/adma.201900353

[18] Zhang F, She L, Jia C, He X, Li Q, Sun J, Lei Z, Liu ZH (2020) Few-layer and large flake size borophene: preparation with solvothermal-assisted liquid phase exfoliation.

RSC Adv 10:27532–27537. https://doi.org/10.1039/D0RA03492D

[19] Zielinkiewicz K, Baranowska D, Mijowska E (2023) Ball milling induced borophene flakes fabrication. RSC Adv 13:16907–16914. https://doi.org/10.1039/D3RA02400H

[20] Su CY, Lu AY, Xu Y, Chen FR, Khlobystov AN, Li LJ (2011) High-quality thin graphene films from fast electrochemical exfoliation. ACS Nano 5:2332–2339. https://doi.org/10.1021/nn200025p

[21] Yang R, Mei L, Zhang Q, Fan Y, Shin HS, Voiry D, Zeng Z (2022) High-yield production of mono-or few-layer transition metal dichalcogenide nanosheets by an electrochemical lithium ion intercalation-based exfoliation method. Nat Protoc 17:358–377. https://doi.org/10.1038/s41596-021-00643-w

[22] Ambrosi A, Sofer Z, Pumera M (2017) Electrochemical exfoliation of layered black phosphorus into phosphorene. Angew Chem Int 56:10443–10445. https://doi.org/10.1002/anie.201705071

[23] Zhang W, Sun L, Nsanzimana JMV, Wang X (2018) Lithiation/delithiation synthesis of few layer silicene nanosheets for rechargeable Li–O2 batteries. Adv Mater 15:1705523. https://doi.org/10.1002/adma.201705523

[24] Yang Y, Leng S, Shi W (2021) Electrochemical exfoliation of porous antimonene as anode materials for sodium-ion batteries. Electrochem Commun 126:107025. https://doi.org/10.1016/j.elecom.2021.107025

[25] Sielicki K, Maślana K, Chen X, Mijowska E (2022) Bottom up approach of metal assisted electrochemical exfoliation of boron towards borophene. Sci Rep 12:15683. https://doi.org/10.1038/s41598-022-20130-w

[26] Chowdhury MA, Uddin MK, Shuvho MBA, Rana M, Hossain N (2022) A novel temperature dependent method for borophene synthesis. Appl Surf Sci Adv 11:100308. https://doi.org/10.1016/j.apsadv.2022.100308

[27] Ambrosi A, Pumera M (2018) Exfoliation of layered materials using electrochemistry. Chem Soc Rev 47:7213–7224. https://doi.org/10.1039/C7CS00811B

[28] Gao LT, Huang P, Guo ZS (2023) Understanding charge-transfer and mass-transfer effects on dendrite growth and fast charging of Li metal battery. J Electrochem Soc 170:050512. https://doi.org/10.1149/1945-7111/acd02b

[29] Wang B, Yin B, Zhang Z, Yin Y, Yang Y, Wang H, Russell TP, Shi S (2022) The assembly and jamming of nanoparticle surfactants at liquid-liquid interfaces. Angew Chem 134:e202114936. https://doi.org/10.1002/anie.202114936

[30] Taşaltın N, Güllülü S, Karakuş S (2022) Dual-role of β borophene nanosheets as highly effective antibacterial and antifungal agent. Inorg Chem Commun 136:109150. https://doi.org/10.1016/j.inoche.2021.109150

[31] Bilgiç G, Korkmaz N, Şahin M, Karadağ A (2022) Synthesis, structural, and electrochemical properties of boron-based ionic liquid. Ionics 28:3289–3300. https://doi.org/10.1007/s11581-022-04575-7

[32] Kudelski A, Bukowska J, Janik-Czachor M, Grochala W, Szummer A, Dolata M (1998) Characterization of the copper surface optimized for use as a substrate for surface-enhanced Raman scattering. Vib Spectrosc 16:21–29. https://doi.org/10.1016/S0924-2031(97)00049-0

[33] Parakhonskiy G, Dubrovinskaia N, Bykova E, Wirth R, Dubrovinsky L (2011) Experimental pressure-temperature phase diagram of boron: resolving the long-standing enigma. Sci Rep 1:96. https://doi.org/10.1038/srep00096

[34] Rohani P, Kim S, Swihart MT (2016) Boron nanoparticles for room-temperature hydrogen generation from water. Adv Energy Mater 6:1502550. https://doi.org/10.1002/aenm.201502550

[35] Noei H, Qiu H, Wang Y, Löffler E, Wöll C, Muhler M (2008) The identification of hydroxyl groups on ZnO nanoparticles by infrared spectroscopy. Phys Chem Chem Phys 10:7092–7097. https://doi.org/10.1039/B811029H

[36] Lu YW, Du XW, Sun J, Han X, Kulinich SA (2006) Influence of surface Si–Ag bonds on photoluminescence of porous silicon. J Appl Phys 100:063512. https://doi.org/10.1063/1.2353397